The mechanism of hydration of MgO-hydromagnesite blends

C. Kuenzel, F. Zhang, [a]V. Ferrándiz-Mas, C.R. Cheeseman*, E.M. Gartner

Department of Civil and Environmental Engineering, Imperial College London,
South Kensington Campus, London SW7 2AZ, United Kingdom,
[a] Department of Architecture and Civil Engineering, University of Bath, BA2 7AY, United Kingdom

*Corresponding author: Email: c.cheeseman@imperial.ac.uk

ABSTRACT

The hydration of reactive periclase (MgO) in the presence of hydromagnesite ($Mg_5(CO_3)_4(OH)_2{\cdot}4H_2O$) was investigated by a variety of physical and chemical techniques. Hydration of pure MgO-water mixtures gave very weak pastes of brucite ($Mg(OH)_2$), but hydration of MgO-hydromagnesite blends gave pastes which set quickly and gave compressive strengths of potential interest for construction applications. The strengths of the blends increased with hydration time at least up to 28 days, and were not significantly decreased by increasing the hydromagnesite content up to 30%. Raman spectroscopy suggests that an amorphous phase, of composition between that of brucite, hydromagnesite and water, may form. Small amounts of calcite also form due to CaO in the MgO source. Thermodynamic calculations imply that the crystalline phase artinite ($MgCO_3{\cdot}Mg(OH)_2{\cdot}3H_2O$) should be the stable product in this system, but it is not observed by either XRD or FTIR techniques, which suggests that its growth may be kinetically hindered.

***Keywords*:** MgO, cement, hydration, hydromagnesite, artinite, brucite,

1. Introduction

MgO (periclase) reacts with water to give brucite ($Mg(OH)_2$) under conditions relevant to normal construction materials. The rate of reaction increases as the crystallinity of the periclase decreases (i.e. smaller mean crystallite size). Periclase is usually manufactured by calcination (decarbonation) of magnesite ($MgCO_3$) that is obtained from natural mineral deposits. The lower the decarbonation temperature, the lower the degree of crystallinity of the resulting periclase. Lightly-burned magnesite is of particular interest for use in hydraulic cements because it reacts very rapidly with water [1].

The hydration of MgO has been extensively studied [2-6]. Water molecules, even from the vapour phase, react rapidly with the anhydrous MgO surface to form a surface layer of $Mg(OH)_2$, but with a structure probably significantly different from that of brucite due to interactions with the underlying oxide. This surface hydrate displays an apparent solubility somewhat higher than pure brucite. Thus, at high relative

humidity, when significant amounts of physically adsorbed water, or excess liquid water, is present, this hydrated surface layer can dissolve in the mobile water layer and reprecipitate as brucite crystallites further away from the surface. The hydrated surface layer on the oxide is continually reformed by further reaction of the underlying oxide with water. The hydration rate of MgO is effectively limited by the rate at which the $Mg(OH)_2$ layer on the surface of the MgO dissolves in the water layer. This in turn is influenced by the rate at which dissolved Mg^{++} and OH^- ions are removed from the water layer by, for example, precipitation.

Periclase can also react with CO_2 in the presence of water (liquid or vapour) to give hydrated carbonates or hydroxy-carbonates such as nesquehonite ($MgCO_3 \cdot 3H_2O$) and hydromagnesite ($Mg_5(CO_3)_4(OH)_2 \cdot 4H_2O$). It is reported that nesquehonite forms readily from aqueous solutions at ambient temperature [9,10]. Table 1 lists the known phases in the MgO-CO_2-H_2O system under conditions of interest, and gives standard free energies of formation from the elements at 25°C [7, 8]. From this data it can be shown that under ambient atmospheric conditions, all hydrated magnesium (hydroxy-) carbonates should convert to magnesite. However, the kinetics of magnesite growth is very slow, especially below 100°C, and so the hydrated carbonates and hydroxy-carbonates, which have much higher growth rates, usually form and do not convert substantially to magnesite over decades under typical exposure conditions for construction materials [11].

Sealed samples of pure pastes of reactive MgO and water do not gain any significant compressive strength, despite the formation of brucite. Moreover, if such pastes are left in the open air, they only carbonate very slowly and do not harden (unlike pastes made of lime, which harden rapidly by atmospheric carbonation - the basis of the lime mortar technology used for many millennia). For this reason, MgO has not until recently been considered of value in simple binders except when significant amounts of other inorganic chemicals are added (e.g. chlorides, sulfates, or phosphates: to make magnesium oxy-chloride, magnesium oxy-sulfate or magnesium phosphate cements, respectively). However, over the last decade or so, there has been increasing interest in using MgO in silicate-based binder system, or in carbonated binders. Blends of MgO with Portland cement, granulated blast furnace slag (GBFS) or coal fly ash (FA) have been studied to produce low-carbon hydraulic binders [1-5,9]. However, there is little evidence for significant contribution of MgO hydration to the strength development of such cements. MgO hydration is also known to cause harmful expansion in Portland cement concretes [10] under certain conditions. Moreover, the fact that conventional MgO production methods are very energy and CO_2 intensive makes it difficult to justify the use of MgO in low-carbon hydraulic cements [12]. A more promising approach for CO_2 emissions reduction is to use MgO in cements that hardens by carbonation, [6-8], but even then, only a fraction of the CO_2 released during manufacture is recaptured. The most desirable approach would be to use MgO derived from natural magnesium silicate raw materials by a new low-energy route, as first proposed by Vlasopoulos [13], but

no practical low-energy production process for achieving this goal yet exists [12]. However, developing such a process remains an important long-term research goal.

A significant advance in developing low-carbon hydraulic cements based on MgO was made in 2009, when the addition of hydrated magnesium carbonates was found to significantly change the hydration of MgO, resulting in pastes that rapidly set and developed significant strength [14-16]. These findings were unexpected and novel [19]. The results have been confirmed for mixtures containing hydromagnesite (HY) as the additive at up to 50% MgO replacement levels [14-16]. The fact that cements made from such mixtures contain significant levels of carbonate is the key to reducing the carbon footprint [12]. The addition of HY reportedly results in more rapid and extensive dissolution of MgO and the precipitation of $Mg(OH)_2$ in the form of very small interlocking crystallites with different morphology from that formed when just MgO is hydrated[16]. However, the reason for this change in morphology, and how it leads to strength development, is still unclear. An improved understanding of the hydration reaction mechanism is essential if these magnesium hydroxy-carbonate cements are to be further developed and optimised. This paper reports on a systematic investigation into the hydration reactions of MgO in the presence of hydromagnesite in order to improve understanding of the hydration mechanism and strength development.

2. Materials and Methods

2.1 Materials

A commercial MgO powder prepared by calcining magnesite at 900°C (Baymag 30, Baymag Inc., Alberta, Canada) and technical grade hydromagnesite (Calmag CALMAGS GmbH, Germany) were used in all experiments. The chemistry of the raw materials is given in Table 2. XRF results are presented as total mass percentage of non-volatile elemental oxides in the material (i.e. on an ignited basis.) The measured and expected loss on ignition (LoI) data are included to demonstrate the purity of each powder. The particle size distribution of the as-received raw materials are given in Fig. 1.

2.2 Preparation of samples

MgO and HY were mixed at mass ratios of 9:1, 8:2 and 7:3. Water was added to form pastes using the recommended mixing method for mortar and pastes [17]. A water/total solids mass ratio of 0.62 was used in all samples. This was the minimum water content that allowed formation of a homogenous paste in all cases, although increasing the hydromagnesite content always increased paste viscosity. Pastes were cast into 50 x 10 x 10 mm rectangular moulds and vibrated for 5 minutes to remove air bubbles. They were then covered with a glass plate to prevent moisture loss and limit reaction with atmospheric CO_2, and allowed to hydrate for 24 hours at 22 ± 1ºC. The samples were then de-moulded and stored in deionised water at 22 ± 1ºC for periods up to 56 days.

2.3 Physical/chemical properties

The heat of hydration of trial mixes was monitored by isothermal conduction calorimetry (Wexham Developments Ltd, UK). The bath temperature was set at 20.0 ± 0.1ºC and 25g of paste samples with 0.62 w/s ratio were mixed by hand for 2 minutes before being placed in the calorimeter. The time between the start of mixing and obtaining the first calorimetry data point was ~10 minutes.

Cured cast samples were removed from the water bath, cut in half to give 25 x 10 x 10 mm prisms and immediately tested in uniaxial compression, parallel to the long axis at a constant loading rate of 0.08 kN/s (ADR Auto strength machine, ELE International, UK) to give compressive strength data. Preliminary tests demonstrated that this non-standard test procedure gave highly reproducible results.

The pH of slurry samples made with a w/s ratio of 3 was determined using an Inlab Routine Pro electrode, (Mettler Toledo, Switzerland). The slurry was continuously stirred while exposed to the atmosphere, and the pH measured at various times throughout the hydration process at 22 ± 1 ºC.

2.4 Microstructural and phase analysis

Powder x-ray diffraction (XRD) using Cu Kα radiation in the range of 5 to 65º 2θ was used to semi-quantitatively compare the relative amounts of crystalline phases in paste samples (X-Pert PRO MPD, PANalytical, Netherlands). Fourier transform infrared spectroscopy (FTIR) was used to detect additional phases in the reaction products. Brucite control samples were prepared by hydrating MgO (Baymag 30) in distilled water. Raman spectrometry (Renishaw inVia Raman Microscope, UK) was used to characterise the different MgO/HY mixes. The microstructures of the as-received powder materials and hydrated, fractured MgO/HY samples were analysed using scanning electron microscopy (SEM, JEOL JSM 5610, Japan). SEM samples were gold coated using a current of 20 mA.

Prior to analysis the paste samples were ground with acetone in a mortar and pestle to inhibit further hydration. This is an accepted way to inhibit hydration of calcium silicate-based cements as hydration water is replaced by acetone [18]. The slurry formed was then filtered and rinsed with additional acetone using vacuum filtration and the solid residue dried at 60 °C to constant weight.

3. Results

3.1 Physical properties

Isothermal conduction calorimetry power output and total heat evolution curves for pastes of pure MgO and a 9:1 MgO: HY blend are shown in Fig. 2. The inclusion of 10% HY greatly accelerates the early hydration compared to pure MgO paste. Hydration occurs prior to obtaining the first calorimetry data point. Both samples show an acceleration period followed by a reducing rate of hydration, suggesting a nucleation and growth process in which the added HY acts as growth sites for hydrates. The maximum

hydration rate occurs after about 10 hours for pure MgO and 2 hours for the sample with 10% HY. The total heat curves may not be very accurate due to the loss of heat in the first few minutes, due to external mixing, and the well-known problem of calibration and baseline drift in long-term isothermal calorimetry experiments, but they appear to indicate that the pure MgO hydrates to a significantly greater extent than the MgO in the 9:1 blend over the one week (168 hours) period shown. Thermodynamic data bases give a heat of hydration of MgO of about 930 J/g [19], so the total heat evolution data suggests that pure MgO is only about 50% hydrated after one week, and the blended MgO is even less hydrated.

Fig. 3 shows the variation in solution pH over 28 days for w/s = 3 slurries of pure MgO, pure HY and a 9:1 MgO: HY mixture. Slurries made with 8:2 and 7:3 MgO: HY mixtures gave similar results to the 9:1 mixture, so the data for these are not shown. The initial pH value for the pure MgO and the MgO: HY mixtures was about 12.4 whereas for pure HY it was close to 10. The pure MgO slurry shows a slow reduction in pH with time, reaching a value of about 11.2 after one week, whereas MgO: HY mixes all showed a much more rapid decrease in pH, reaching values close to, or even slightly below, those of pure HY after ~1 day.

Table 3 shows that all three MgO-HY paste samples give very similar compressive strength development, achieving about 18 MPa after 7 days, and increasing to about 24 MPa at 28 days. Pure MgO pastes did not give sufficient strength for sample demoulding and so cannot be compared directly in the table.

3.2 Microstructural and phase analyses

The XRD scans shown in Fig. 4 are only semi-quantitative, as there were no internal standard. However, given that the sample preparation and analysis techniques were quite repeatable, comparisons of peak intensities seem justifiable as a way of examining changes in the relative amounts of the main crystalline phases present. In the pure system, (Fig. 4b) periclase disappears (dissolves) with time while brucite forms (precipitates). Even after 28 days of hydration, the periclase peak in the pure system has not completely disappeared. A weak peak in Fig. 4a also indicates the formation of some calcite ($CaCO_3$). CaO is an impurity in the MgO that carbonates by reaction with atmospheric CO_2.

The reactions of MgO: HY blends show similar trends as a function of hydration time, with the disappearance of periclase and formation of brucite, but at different rates, as clearly shown in Fig 4c for pure MgO and 9:1 MgO: HY pastes hydrated for 28 days. Significantly more MgO appears to have hydrated and more $Mg(OH)_2$ has formed in the pure paste than in the 9:1 blend. In addition, the $Mg(OH)_2$ peak in the 9:1 blend is significantly broader than in the pure system, suggesting a smaller mean crystallite size [20]. This is in agreement with calorimetry data, where MgO does not fully hydrate to brucite.

In the XRD data for MgO: HY blends, HY peaks were observed mainly for samples with MgO: HY ratios of 8:2 and 7:3 but hardly at all for the 9:1 samples due to the low concentration of HY and the corresponding weak diffraction peaks. $Mg(OH)_2$ and MgO were always present, as expected, and the $Mg(OH)_2$ peak always shows significant broadening compared to those found in the pure system. No additional peaks are observed, so any other phases which might be present must be effectively x-ray amorphous.

The FTIR spectra of samples produced by hydrating MgO, HY and the MgO: HY 70:30 mix for 28 days are shown in Fig. 5. The MgO: HY mixes with ratios of 90:10 and 80:20 are not shown because HY is only present in small quantities and the corresponding bands are too weak to observe [21]. Several bands can be detected which have been characterised in previous studies, as shown in Table 4. All the bands identified are seen in the spectra for the three samples containing HY, except for that due to O-H bonds in $Mg(OH)_2$ at 3700 cm^{-1} which are, as expected, not observed in the pure HY sample. Small amounts of carbonate are observed in hydrated MgO. This is consistent with the XRD data and confirms that the MgO reacts with atmospheric CO_2 over time, although the carbonate ions detected in this case are probably mainly present as $CaCO_3$. The presence of carbonate impurities in brucite ($Mg(OH)_2$) has previously been reported in FTIR studies [22]. Previous research has shown that for pure magnesite, ($MgCO_3$), a single asymmetric stretching band is observed between 1478 and 1450 cm^{-1}. The presence of two bands in the 1420-1480 cm^{-1} region, as in HY, indicates the presence of two different carbonate ion environments [21, 23, 24]. The HY signal at ~600cm^{-1} is unassigned, although this band has been observed by other researchers [25]. Studies on the dehydration and rehydration of HY have also identified a band at ~2350cm^{-1} which has been assigned either to a CO_2 inclusion or a terminal CO_2, corresponding to the v_3 fundamental of CO_2 [25, 26]. However, this band cannot be measured in our study, probably due to the background noise level.

Raman spectroscopy was used to search for other phases not 'visible' using FTIR. Fig. 6 shows the Raman spectra of pure HY, hydrated MgO, hydrated MgO: HY samples with ratios of 9:1 and 7:3. All samples had been cured for 28 days. Three main peaks at 280 cm^{-1}, 440 cm^{-1} and 1100 cm^{-1} can be identified. The peaks at 280 cm^{-1} and 440 cm^{-1} observed in the hydrated MgO sample also appear in the other spectra except for the spectrum of HY. These two peaks are related to $Mg(OH)_2$ [27]. The peak at ~1120cm^{-1} is due to symmetrical stretching of the CO_3^{2-} ion, [28, 29], which is why it is much stronger in Raman spectra. However, of more interest is the formation of a broad weak peak or series of small peaks between 1050 and 1120 cm^{-1} for MgO: HY mixes. These peaks are not seen for pure MgO and HY and are probably due to symmetrical stretching of CO_3^{2-} in other magnesium carbonate phases, which could be very poorly crystalline. Table 5 lists a number of possible phases with peaks in this range.

Fig. 7 shows SEM images of hydrated MgO and HY and fracture surfaces of pastes cured for 7 and 28 days. Fig. 7 (c, d, e and f) show that over time well-developed crystalline morphologies (plates) are formed. These are not observed either in hydrated pure MgO or in pure HY samples.

4. Discussion

The initial rate of hydration of MgO is strongly increased by HY, which suggests that HY additions provide additional growth sites for the hydrates ($Mg(OH)_2$ and probably other x-ray amorphous hydrate phases) promoting further MgO hydration [13]. It was expected that pure MgO would fully hydrate to $Mg(OH)_2$, but this was not shown by calorimetry or XRD. This incomplete hydration is probably due to a brucite layer forming on the MgO particle surface that inhibits water reaching unreacted MgO by acting as a passivation layer. However, it is expected that eventually pure MgO will fully hydrate to $Mg(OH)_2$. Of particular interest is the high initial pH of 12.4 for MgO and MgO: HY systems when mixed with water, because a pH of ~10 had been expected. The measured pH is actually close to that of a saturated portlandite ($Ca(OH)_2$) solution, leading to the conclusion that CaO impurities in the MgO and HY cause the high initial pH. The pH of the pure MgO slurry then falls slowly with time due to atmospheric carbonation to produce calcite, consistent with XRD observations of calcite in the system. When MgO is mixed with HY, the pH falls much more rapidly, which can be explained by HY containing readily soluble carbonate ions which are capable of neutralizing $Ca(OH)_2$ much more rapidly than CO_2 from the atmosphere. Rapid precipitation of calcite at early ages due to reaction with HY could provide another source of nucleation sites for hydration products of MgO and the formation of $CaCO_3$ may also contribute to rapid setting and compressive strength development.

After the first peak in the calorimetry data, the rate of heat evolution is significantly lower for the MgO: HY blends, and the XRD data confirm that the amount of unreacted MgO is higher in these blends at later ages than in the pure system, despite the fact that blends give far higher compressive strengths. This suggests that additional hydrates produced in the blends have a retarding effect on the later hydration of MgO. The effect might be due to surface blocking or to the formation of diffusion barriers. These additional hydrates are also presumed to be responsible for strength development.

Table 1 gives the free energies of the known crystalline phases of interest in this system. Artinite $\{MgCO_3{\cdot}Mg(OH)_2{\cdot}3H_2O\}$ is intermediate in composition between $Mg(OH)_2$ and HY and can, in principle, be formed from these two phases and water by the following reaction:

$$3Mg(OH)_2 + 4MgCO_3{\cdot}Mg(OH)_2{\cdot}4H_2O + 8H_2O \rightarrow 4(MgCO_3{\cdot}Mg(OH)_2{\cdot}3H_2O) \quad (2)$$

A calculation using the thermodynamic data from Table 1 gives the free energy change of the reaction as -6.42 kJ/mol, which implies that the equilibrium should lie on the right-hand side at 25°C. Thus,

artinite should form in MgO: HY blends. However, it is not detected in the XRD data. This could be due to weak XRD peaks or it could be due to a very low degree of crystallinity. Artinite has a carbonate symmetric stretching peak at 1092 cm^{-1} (Table 5) which should be observable in both IR and Raman spectra. No such peak is visible in the FTIR spectra of MgO: HY blends (Fig. 5) but it could be too weak to detect. The Raman spectra of hydrated MgO: HY blends (Fig. 6) show a very broad peak between about 1040 and 1120 cm^{-1} which suggests a disordered hydroxy-carbonate phase that might not be too far from artinite in composition. It thus seems possible that some kind of amorphous hydroxy-carbonate, intermediate in composition between HY and brucite, may form in MgO: HY pastes and be responsible for high compressive strengths relative to pure MgO pastes.

The SEM images in Fig. 7 neither confirm nor deny the hypothesis of a new phase in MgO: HY pastes. It is notable that quite large (~5μm) platy crystals are formed after 28 days in the 9:1 MgO: HY paste. These could be $Mg(OH)_2$, but they are much larger than the crystals observed in pure MgO. Moreover, the XRD peak broadening of brucite observed in the MgO: HY blends would tend to suggest smaller, rather than larger, crystals. It is therefore possible that these crystals are the new phase, in which case the poor x-ray crystallinity is due to either being very thin in the direction perpendicular to the basal plane, or possibly to some other kind of internal disorder.

5. Conclusions

Addition of hydromagnesite, (HY, $Mg_5(CO_3)_4(OH)_2{\cdot}4H_2O$), significantly accelerates the hydration of reactive periclase (MgO) in pastes. The hydration of pure MgO gives very weak pastes despite fairly rapid formation of brucite ($Mg(OH)_2$), but the addition of HY at MgO at replacement dosages of 10-30% results in pastes that give significant compressive strengths, despite the absence of significant increases in the apparent degree of hydration of the MgO. Evidence from pH measurements also suggests that carbonate ions from HY can combine rapidly in solution with calcium ions released by CaO, (an impurity in the MgO source,) to precipitate small amounts of calcite at early ages. This might also contribute to an acceleration of the hardening reactions, perhaps by acting as nucleation sites.

Analyses of the hydrated pastes by XRD and FTIR techniques do not clearly show any new MgO-based phases, but there is a broad but weak Raman peak at 1120-1040 cm^{-1} that could represent a new amorphous phase. It is thus concluded that if any new cohesive phase forms in this system, it is probably X-ray amorphous with a composition roughly intermediate between that of HY and brucite. A thermodynamic calculation suggests that artinite ($MgCO_3{\cdot}Mg(OH)_2{\cdot}3H_2O$) should ~~form~~ be a stable product phase during the hydration of MgO:-HY blends, but the fact that it is not observed by XRD or FTIR suggests that its formation may be kinetically hindered.

The formation of an amorphous phase intermediate in composition between HY, ~~and~~ $Mg(OH)_2$ and water is a possible explanation for the surprisingly high strengths produced by hydrating MgO: HY blends, compared to the very low strengths produced by hydration of pure MgO. Such a phase must have a high degree of cohesion.

These results hold promise for the development of improved binders in the magnesium-hydroxy-carbonate system. Such binders have the potential to reduce carbon emissions from manufacturing construction materials, provided that MgO can be obtained from magnesium silicates by an energy-efficient process. However, there are currently many aspects of hydration and strength development in this system that remain unclear.

Acknowledgement

F. Zhang acknowledges the support of an EPSRC Case Award sponsored by Laing O'Rourke.

References

1. Birchal, V.S.S., S.D.F. Rocha, and V.S.T. Ciminelli, *The effect of magnesite calcination conditions on magnesia hydration.* Minerals Engineering, 2000. **13**(14-15): p. 1629-1633.
2. Birchal, V.S.S, S.D.F. Rocha, M.B. Mansur, and V.S.T. Ciminelli, *A simplified mechanistic analysis of the hydration of magnesia.* The Canadian Journal of Chemical Engineering, 2001. **79**: p. 507-511.
3. Feitknecht, W. and H. Braun, *Der Mechanismus der Hydratation von Magnesiumoxid mit Wasserdampf.* Helvetica Chimica Acta, 1967. **80**.
4. Glasson, D.R., *Reactivity of lime and related oxides (Part VII) - Production of activated lime and magnesia.* Journal of Applied Chemistry, 1963. **13**: p. 111-118.
5. Maryska, M. and J. Blaha, *Hydration kinetics of magnesium oxide: Part 3 hydration rate of MgO in terms of temperature and time of its firing.* Ceramics - Sillicaty, 1997. **41**: p. 121-123.
6. Smithson, G.L. and N.N. Bakhshi, *The kinetics and mechanism of the hydation of magnesium oxide in a batch reactor.* The Canadian Journal of Chemical Engineering, 1969. **47**: p. 508-513.
7. Dean, J.A., *Lange's Handbook of Chemistry*. 15 ed. 1999, New York, USA: McGraw-Hill.
8. Hänchen, M., V. Prigiobbe, R. Baciocchi, and M. Mazzotti, *Precipitation in the Mg-carbonate system—effects of temperature and CO_2 pressure.* Chemical Engineering Science, 2008. **63**: p. 1012–1028.
9. Zhao, L., L. Sang, J. Chen, J. Ji, and H.H. Teng, *Aqueous carbonation of natural brucite, relevance to CO2 sequestration.* Environmental Science Technology, 2010. **44**: p. 406-411.
10. Xiong, Y.L. and A.S. Lord, *Experimental investigation of the reaction path in the MgO-CO2-H2O system in solution with various ionic strenght and their applications in nuclear waste isolation.* Applied Geochemistry, 2008. **23**(6): p. 1634-1659.

11. Saldi, G.D., G. Jordan, J. Schott, and E.H. Oelkers, *Magnesite growth rate as a function of temperature and saturation state.* Geochmica et Cosmochimica Acta, 2009. **73**: p. 5646-5657.
12. Gartner, E. and T. Sui, *Alternative cement clinkers.* Cement and Concrete Research, 2017 (in press - available online.)
13. Vlasopoulos, N., *Waste minimisation through sustainable magnesium oxide cement products*, in *Civil and Environmental Engineering*. 2007, Imperial College London: London.
14. Flatt, R.J., N. Roussel, and C.R. Cheeseman, *Concrete: an eco material that needs to be improved.* Journal of European Ceramic Society, 2012. **32**: p. 2787-2798.
15. Devaraj, A.R., H.X. Lee, D.A.M. Velandia, and N. Vlasopoulos, *Binder Composition*. 2011: US 20140290535 A1.
16. Vlasopoulos, N. and C.R. Cheeseman, *Binder composition*. 2009: US Patent 8496751 B2.
17. BS, *EN 196-1 Methods of testing cements - Determination of strength*. 2005.
18. Collier, N.C., J.H. Sharp, N.B. Milestone, J. Hill, and I.H. Goffrey, *The influence of water removal techniques on the composition and microstructure of hardened cement pastes.* Cement and Concrete Research, 2008. **38**: p. 737-744.
19. Thomas, J.J., S. Musso, and I. Prestini, *Kinetics and activation energy of magnesium oxide hydration.* Journal of the American Ceramic Society, 2014. **97**(1): p. 275-282.
20. Navarro, C.R., F.E. Hansen, and W.S. Ginnell, *Calcium hydroxide crystal evolution upon ageing of lime putty.* Journal of American Ceramic Society, 1998. **81**: p. 3032-3034.
21. Bruni, S., F. Cariati, P. Fermo, A. Pozzi, and L. Toniolo, *Characterization of ancient magnesian mortars coming from northern Italy.* Thermochimica Acta, 1998. **321**: p. 161-165.
22. Frost, R.L. and J.T. Kloprogge, *Infrared emission spectroscopic study of brucite.* Spectrochimica Acta Part A: Molecular and Biomolecular Spectroscopy, 1999. **55**: p. 2195-2205.
23. Choudhari, B.P., M.C. Vaidya, and D.S. Datar, *Physico-chemical studies on basic magnesium carbonates.* Indian Journal of Chemistry, 1972. **10**: p. 731-733.
24. Sawada, Y., J. Yamaguchi, O. Sakurai, K. Uematsu, N. Mizutani, and M. Kato, *Thermal decomposition of basic magnesium carbonates under high-pressure gas atmospheres.* Thermochimica Acta, 1979. **32**: p. 277-291.
25. Botha, A. and C.A. Strydom, *DTA and FT-IR analysis of the rehydration of basic magnesium carbonate.* Journal of Thermal Analysis and Calorimetry, 2003. **71**: p. 987-995.
26. Schrader, B., *Infrared and Raman spectroscopy: methods and applications*. 1989, London: Wiley.
27. Buchanan, R.A., H.H. Caspers, and J. Murphy, *Lattice Vibration Spectra of Mg(OH)2 and Ca(OH)2.* Applied Optics, 1963. **2**(11): p. 1147-1150.
28. Edwards, H.G.M., S.E. Jorge Villar, J. Jehlicka, and T. Munshi, *FT–Raman spectroscopic study of calcium-rich and magnesium-rich carbonate minerals.* Spectrochimica Acta Part A, 2005. **61**: p. 2273-2280.
29. Scheetz, B.E. and W.B. White, *Vibrational spectra of the alkaline earth double carbonates.* American Mineralogist, 1977. **62**: p. 39-50.

30. Han, H., S. Hu, J. Feng, and H. Gao, *Effect of stearic acid, zinc stearate coating on the properties of synthetic hydromagnesite.* Applied Surface Science, 2011. **257**: p. 2677-2682.
31. Raade, G., *Dypingite, a new hydrous basic carbonate of magnesium, from Norway.* The American Mineralogist, 1970. **88**: p. 1457.
32. White, W.B., *Infrared characterization of water and hydroxyl ion in the basic magnesium carbonate minerals.* American Mineralogist, 1971. **56**: p. 46-53.
33. Lanas, J. and J.I. Alvarez, *Dolomitic lime: thermal decomposition of nesquehonite.* Thermochimica Acta, 2004. **421**: p. 123-132.
34. Frost, R.L., S. Bahfenne, and J.E. Graham, *Raman spectroscopic study of the magnesium carbonate minerals- artinite and dypingite.* Journal of Raman Spectroscopy, 2009. **40**(8): p. 855-860.
35. Kontoyannis, C.G. and N.V. Vagenas, *Calcium carbonate phase analysis using XRD and FT-Raman spectroscopy.* The Analyst, 2000. **125**: p. 251-255.

Table 1: Gibbs free energies of formation from the elements in their standard states at 298K for phases of interest to this work. [7, 8]

Phase	chemical composition	ΔG^0_f [kJ mol^{-1}]
Periclase	MgO	-566
Carbon dioxide (gas)	CO_2	-394
Water (liquid)	H_2O	-237
Brucite	$Mg(OH)_2$	-835
Magnesite	$MgCO_3$	-1028
Nesquehonite	$MgCO_3 \cdot 3H_2O$	-1724
Lansfordite	$MgCO_3 \cdot 5H_2O$	-2200
Artinite	$MgCO_3 \cdot Mg(OH)_2 \cdot 3H_2O$	-2569
Hydromagnesite	$(MgCO_3)_4 \cdot Mg(OH)_2 \cdot 4H_2O$	-5865
Calcite	$CaCO_3$	-1129
Aragonite	$CaCO_3$	-1128

Table 2: Chemical composition of MgO and hydromagnesite (HY) used in this study analysed by XRF using powder samples. The non-volatile elements (i.e. excluding CO_2 and H_2O) are assumed to be present as oxides, totalling 100% on an ignited basis. Measured and expected 1000ºC ignition loss values are also given for the actual materials as used.

	sample	
element	HY	MgO
MgO	95.55	92.55
CaO	3.33	1.74
SiO_2	0.47	2.72
Na_2O	0.28	0.76
NiO	0.19	nd
Fe_2O_3	0.11	0.77
Al_2O_3	nd	1.02
SO_3	0.07	0.44
LoI measured	55.60	2.0
LoI expected	56.90	0
BET surface area [m^2/g]	n.a	30

nd = not detected

Table 3: Compressive strengths of paste samples at 7 and 28 days. Means and standard deviations are calculated from 6 replicate measurements.

Time [days]	7		28	
MgO:HY ratio	strength [MPa]	SD	strength [MPa]	SD
9:1	17.3	0.8	24.6	0.6
8:2	17.1	0.9	23.8	0.7
7:3	17.3	1.0	24.5	0.4

Table 4: Summary of the bands detected and their origins, for the FTIR spectra in Fig.5**.**

Band position (cm^{-1})	**origin**	**movement**	**reference**
~ 600	Unknown	Unknown	[25, 26]
800 - 880	CO_3^{2-} from HY	Bending vibrations	[23, 30]
1120	CO_3^{2-} from HY	V_1 symmetric stretching vibration	[23, 30]
1420 - 1480	CO_3^{2-}/ $HCO_3^-$from HY	V_3 asymmetric stretching vibration	[23, 24, 30]
1650 (shoulder)	H_2O	Bending vibration	[31, 32]
3450, 3510	HY water of crystallisation		[23, 30]
3650	$Mg(OH)_2$ from HY	Free O-H vibration	[23, 33]
3700	$Mg(OH)_2$	Anti-symmetrical O-H stretching vibration of lattice hydroxide	[22, 23]

29 Table 5: Bands summary of different hydrated magnesium carbonates as well as selected
30 calcium carbonates in the region of 1200 - 1000 cm^{-1} [28, 34, 35].
31

Mineral name	chemical formula	Wavenumber [cm^{-1}]
Artinite	$Mg_2(OH)_2CO_3 \cdot 3H_2O$	1092
Dypingite	$Mg_5(CO_3)_4(OH)_2 \cdot 5H_2O$	1120
Dolomite	$CaMg(CO_3)_2$	1098
Huntite	$Mg_3Ca(CO_3)_4$	1123
Hydromagnesite	$Mg_5(CO_3)_4(OH)_2 \cdot 4H_2O$	1119
Magnesite	$MgCO_3$	1094
Nesquehonite	$Mg(HCO_3)(OH) \cdot 2(H_2O)$	1100
Calcite	$CaCO_3$	1084
Aragonite	$CaCO_3$	1084
Vaterite	$CaCO_3$	1089
-	HCO_3^-	1017
-	CO_3^{2-}	1065

32
33

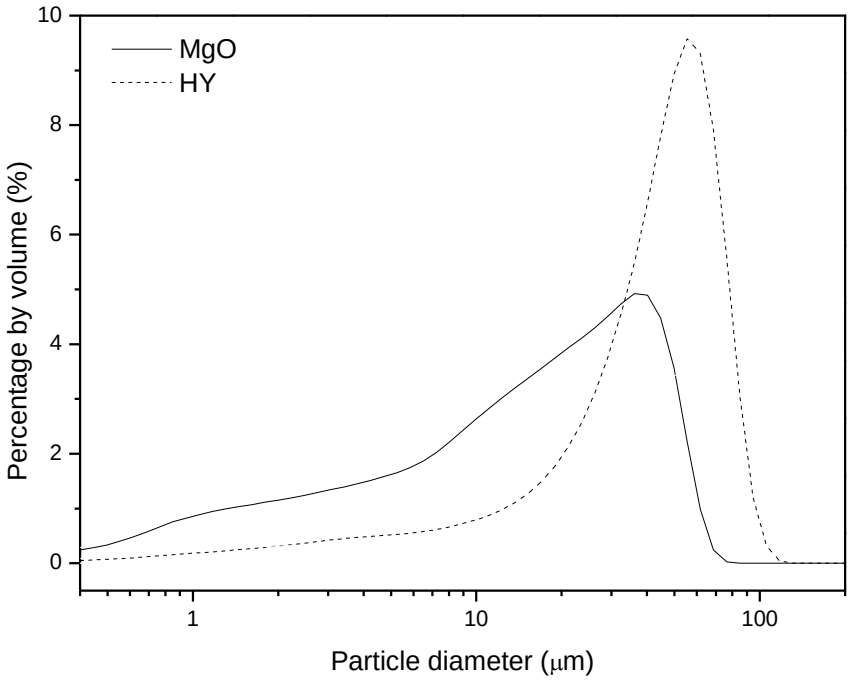

Fig. 1. Particle size distributions of the MgO and hydromagnesite (HY) used in this research.

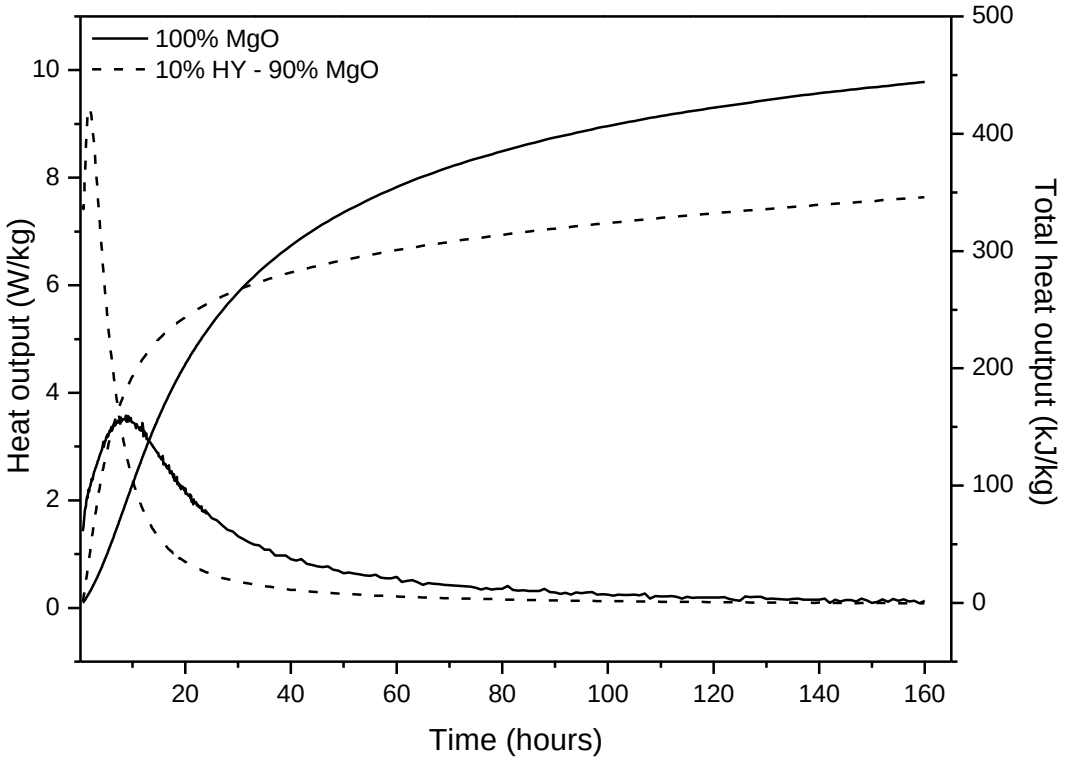

Fig. 2. Isothermal conduction calorimetry data for the pure MgO and 9:1 MgO: HY pastes. Heat output is per kg of total sample mass.

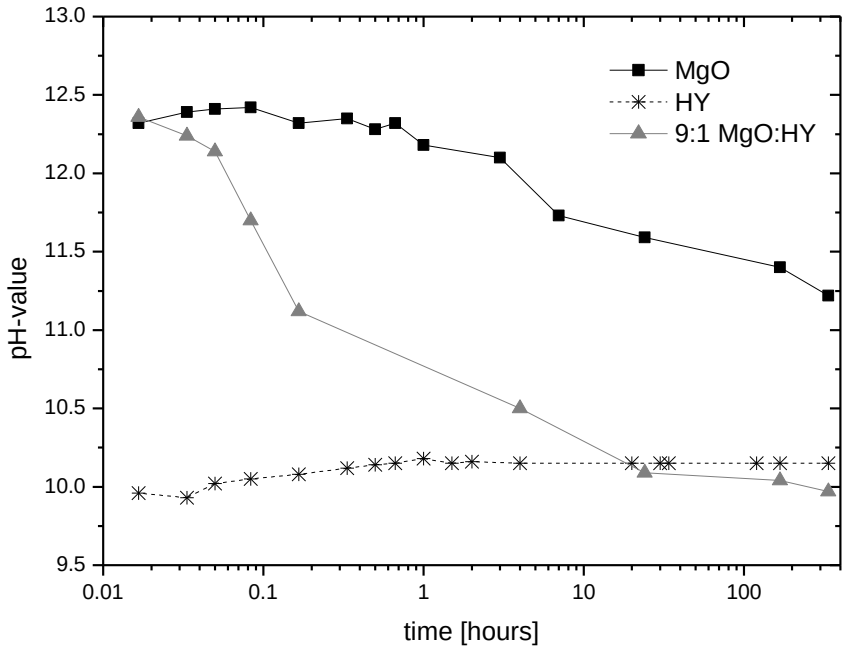

Fig. 3. Change in solution pH over time of w/s = 3 slurries containing 100% MgO, 100% HY and 10% HY - 90% MgO mixes. Each point represents the average of two measurements.

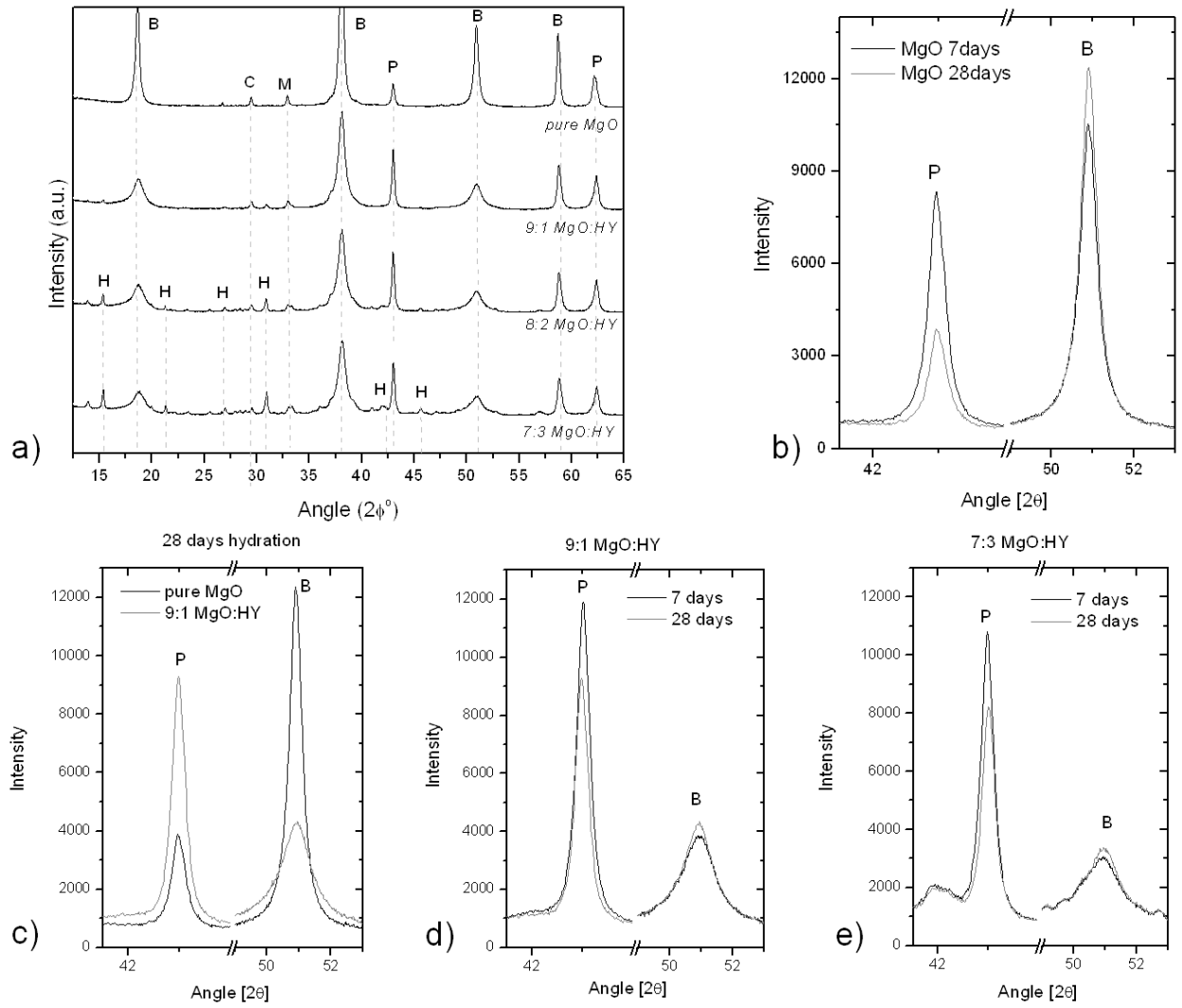

Fig. 4. Powder XRD scans of hydrated MgO and MgO-HY pastes made at 0.62 initial w/s ratio. a) full scans of all four samples after 28 days curing; b) comparison of main periclase and brucite peaks for pure MgO pastes at 7 and 28 days; c) Comparison of the main periclase and brucite peaks for pure MgO and 9:1 MgO: HY mixture after 28 days; d) Comparison of the main periclase and brucite peaks for the 9:1 MgO: HY mixture after 7 and 28 days; e) Comparison of the main periclase and brucite peaks for the 7:3 MgO: HY mixture after 7 and 28 days. Key: B = brucite [$Mg(OH)_2$], C = calcite [$CaCO_3$], H = hydromagnesite [$Mg_5(CO_3)_4(OH)_2.4H_2O$], M = magnesite [$MgCO_3$] and P = periclase [MgO].

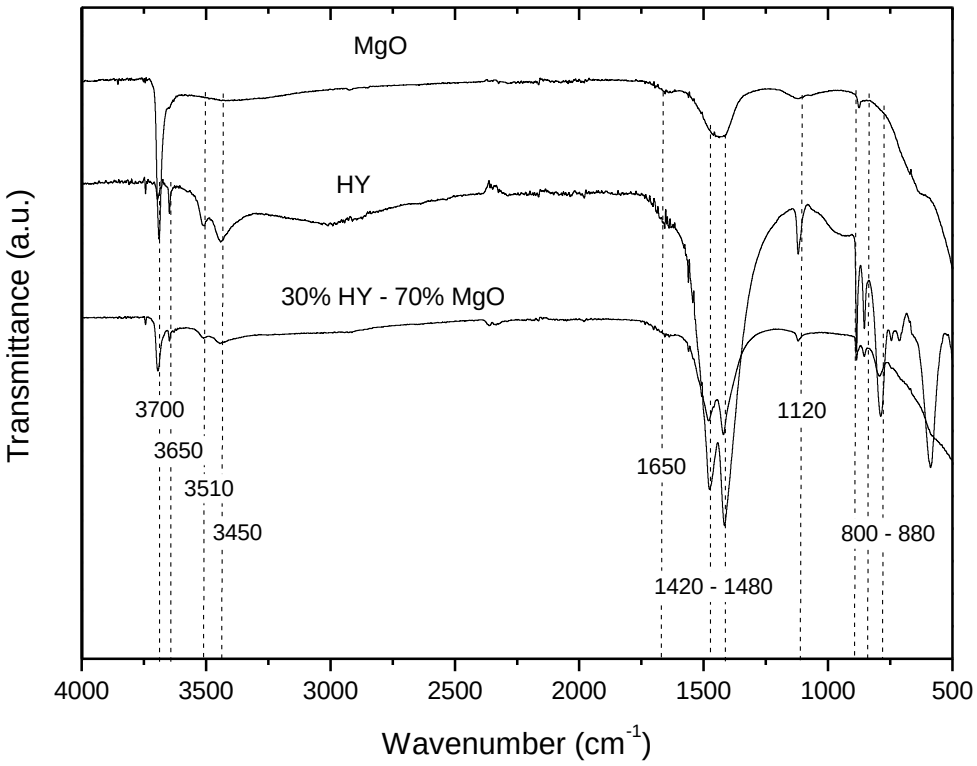

55
56

57 **Fig. 5.** FTIR spectra of pure MgO and 3:7 HY: MgO paste hydrated for 28 days, and HY as
58 used. The peaks of interest are indicated with dotted lines and their wave number labelled.

59

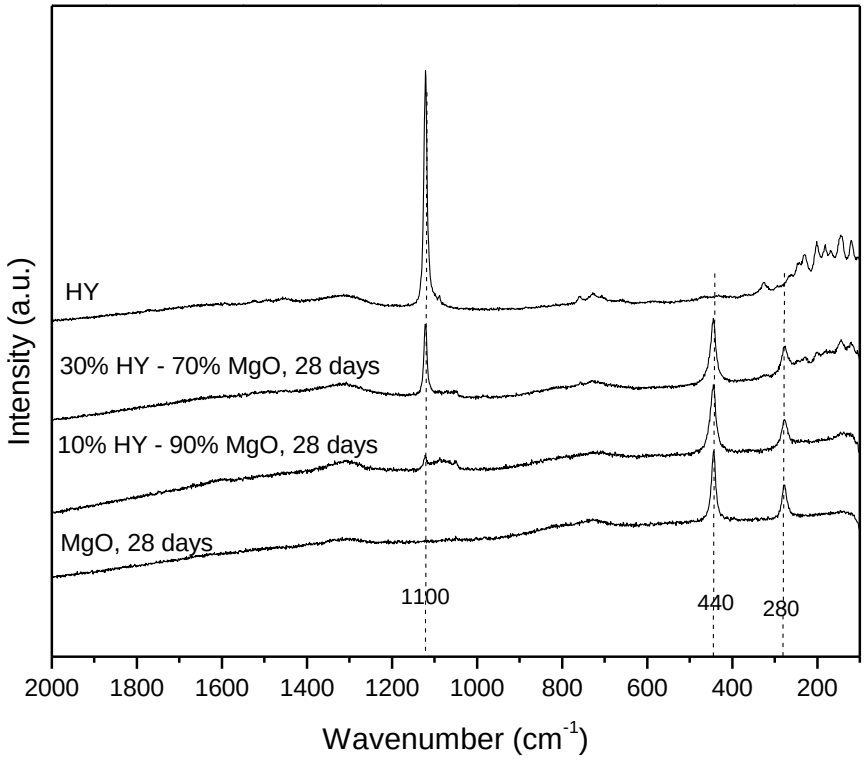

Fig. 6. Raman spectra of the HY sample as used; plus the pastes of 3:7 and 9:1 HY: MgO blends, and pure MgO, hydrated for 28 days.

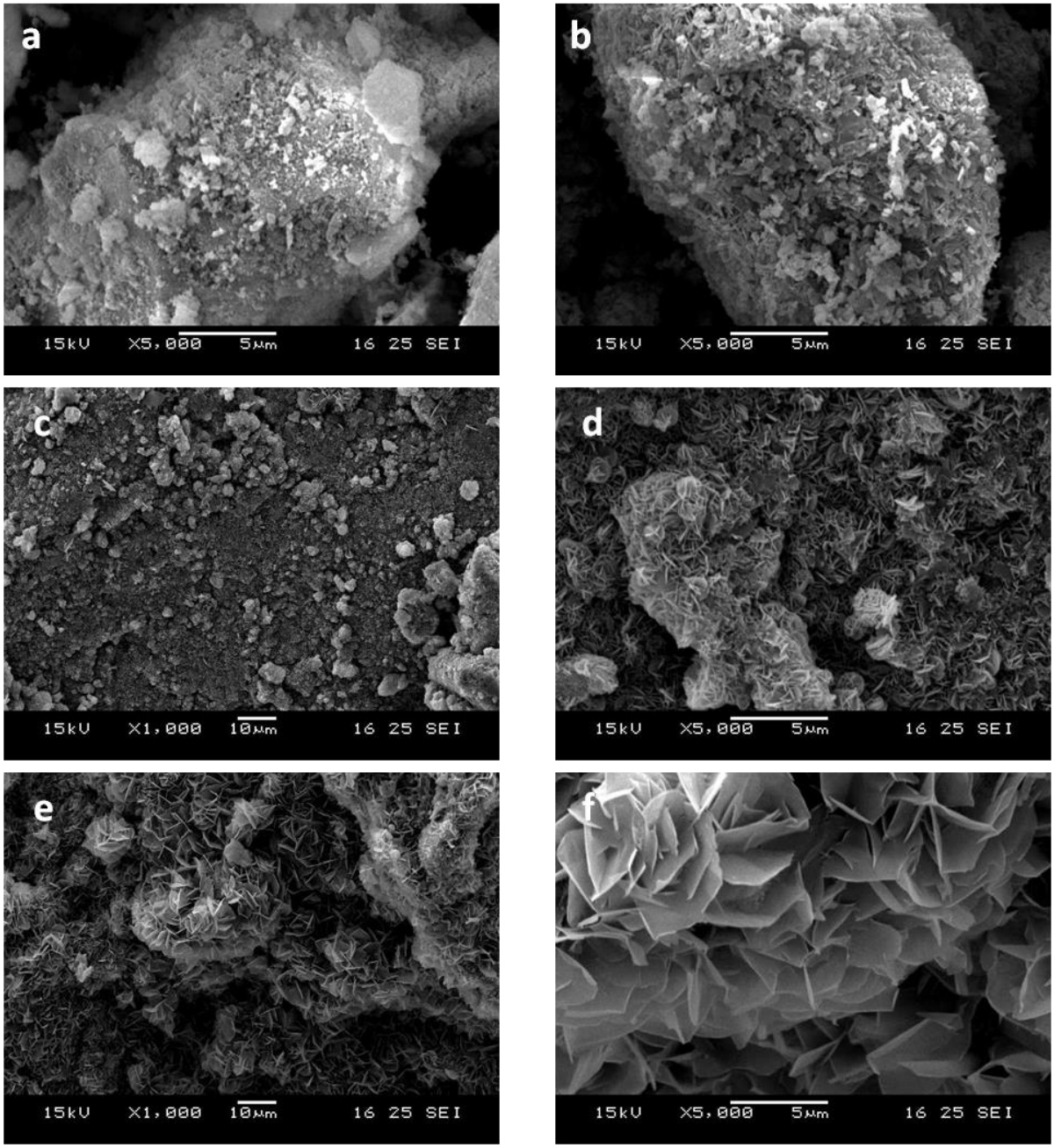

Fig. 7. SEM images of a) as-received MgO; b) as-received HY sample; c and d) 9:1 MgO: HY pastes after 7 days hydration; e and f) 9:1 MgO: HY pastes after 28 days hydration.